Arabian Journal of Chemistry (2022) **15**, 103637

King Saud University

Arabian Journal of Chemistry

www.ksu.edu.sa
www.sciencedirect.com

ORIGINAL ARTICLE

Removal of Fe^{3+} from ammonium dihydrogen phosphate solution in an impact-jet hydraulic cavitation extractor

Yan Cao [a,b], Xiaowei Liu [a], Xian'e Ren [a,b], Yongchun Huang [a,b,*]

[a] *Department of Biological and Chemical Engineering, Guangxi University of Science and Technology, Liuzhou, Guangxi 545006, PR China*
[b] *Guangxi Key Laboratory of Green Processing of Sugar Resources (Guangxi University of Science and Technology), Liuzhou, Guangxi 545006, PR China*

Received 10 October 2021; accepted 9 December 2021
Available online 14 December 2021

KEYWORDS

Extraction;
Hydraulic cavitation;
Ammonium dihydrogen phosphate;
Fe^{3+};
Equilibrium equation

Abstract The impurity of Fe^{3+} in ammonium dihydrogen phosphate (MAP) solution has a significant influence on the morphology and quality of products. The removal of Fe^{3+} from the MAP solution by Di-(2-ethylhexyl) phosphoric acid (D2EHPA) was investigated in an impact-jet hydraulic cavitation (HC) extractor. The organic phase and aqueous phase can be highly mixed under the action of hydraulic cavitation. The extraction efficiency of 80% can be achieved when the extraction reaction was carried out for only 5 min. It was found that the extraction of Fe^{3+} with D2EHPA was an exothermic reaction, and the equilibrium equation of extraction was obtained by slope method as follows: $Fe^{3+}_{(aqu)} + 8(HD)_{2(org)} = (FeD_3 \cdot 13HD)_{(org)} + 3H^{+}_{(aqu)}$

After the two-stage extraction, the extraction efficiency of up to 96.7% can be reached (only 3.4 ~ 4 ppm Fe^{3+} remained in the aqueous phase), and the MAP crystals with regular polyhedral structure, single phase nature, and high optical transmittance were obtained.

1. Introduction

Ammonium dihydrogen phosphate (MAP) is an important fine phosphate product, which is widely used in agriculture (Gupta et al., 2014), food (Lampila, 2013), fire protection (Kong et al., 2018), and electro-optic materials (Xue et al., 2005). There are three main methods for the production of MAP in industry, which are the methods of thermal-process phosphoric acid, wet-process phosphoric acid (WPA), and urea phosphate mother liquid. In recent years, the wet-process phosphoric acid method has been paid more attention due to its advantages of low cost,

* Corresponding author at: Department of Biological and Chemical Engineering, Guangxi University of Science and Technology, Liuzhou, Guangxi 545006, PR China.
E-mail address: huangyc@yeah.net (Y. Huang).
Peer review under responsibility of King Saud University.

Production and hosting by Elsevier

https://doi.org/10.1016/j.arabjc.2021.103637

low energy consumption and low pollution. However, MAP produced by WPA method contains many impurities, such as Fe^{3+}, Al^{3+}, Mg^{2+}, SiF_6^{2-}, and SO_4^{2-}, etc. (El-Bayaa et al., 2011). These impurities, especially for Fe^{3+}, have a certain wrapping effect on the crystal particles, which can change the crystal growth rate. The crystal morphology and purity of the MAP product can be affected by impurities, which leads to the reduction of the quality of MAP product. Therefore, it is necessary to remove these impurities by some method, such as solvent extraction (Li et al., 2020), membrane separation (Luo et al., 2014), and adsorption (Zhu et al., 2017), etc., before the MAP solution is concentrated. The solvent extraction is a traditional and widely used method to remove impurities in the phosphate industry (Lo et al., 1983; Luo et al., 2009; Mohammad et al., 1997). Luo et al. (2011) have studied the removal of Mg^{2+} from MAP solution by solvent extraction. It was pointed out that superior grade MAP can be obtained by three-stage extraction. However, the traditional extraction equipment had obvious amplification effect and the extraction efficiency was needed to be further improved. Fan et al. (2020) proposed a rotating microchannel extractor, in which Fe^{3+} was removed from MAP solution with P507. The air was introduced into microchannel device to further strengthen the extraction of Fe^{3+}. It was pointed out that the extraction efficiency of Fe^{3+} was up to 97.9% by two-stage extraction. Although the microchannel equipment had excellent extraction performance, its processing flux was small and there were some difficulties in equipment integration and amplification.

Hydraulic cavitation (HC) (Panda et al., 2020) is a green and efficient treatment technology, which is widely used in food processing, environmental pollution control, and drug synthesis, etc. More and more scholars' attention has been attracted by HC due to its advantages of low energy consumption, low cost, easy control and industrial amplification. The effects of HC include chemical effect (free radical effect) and physical effect (mechanical shear effect) (Panda et al., 2019; Yan et al., 2020), which are generated based on cavitation elements, such as orifice plate, venture, throttling valve, etc. The effects of HC are mainly reflected in two aspects (Panda et al., 2018). On the one hand, instantaneous high temperature, high pressure and free radicals are generated during the cavitation bubbles collapse, which can strengthen the chemical reaction process. On the other hand, the strong shock wave and high-speed micro-jet flow are produced, which can strengthen the contact of substances and accelerate the mass transfer process in the flow field. Because of the above characteristics, HC is favored in biofuel synthesis, wastewater treatment, emulsification, and extraction, etc. Maddikeri et al. (2014) have studied the synthesis of biodiesel from waste cooking oil by three different HC reactors. The results showed that the maximum yield was obtained by the slit venturi reactor, and the higher yield was obtained by HC method compared to ultrasound and conventional method. It was attributed to the micro-scale turbulence caused by the cavitation effect. Rajoriya et al. (2017) have studied the decolorization of RBI3 dye by HC. The excellent decolorization can be achieved by using a combination of HC and ozone. Saxena et al. (2018) proposed to use hybrid HC (such as HC + O_3, HC + H_2O_2 and HC + Fenton's reagent) to degrade organic pollutants in tannery waste effluent. It was shown that the process of HC combined with Fenton's reagent was the most efficient and energy-saving hybrid process. Ramisetty et al. (2014) reported the stable submicron emulsions of coconut oil in water can be obtained by using venturi-based HC reactor. The minimum droplet size of 170 nm was obtained. The size of droplet generated in slit venturi reactor was smaller than that in the circular venturi reactor. Based on hydraulic cavitation technology, the essential molecules, such as the proteins and lipids, can be effectively extracted from natural products. Table 1 shows some substances extracted by using venturi-based or orifice-based HC devices reported by some researchers. Generally, HC technology has a very wide range of applications. However, there are few reports on the extraction of metal ions by HC technology.

On the basis of the excellent mixing effects of HC, it was proposed that removal of Fe^{3+} from MAP solutions by using HC technology in this paper, and an impact-jet hydraulic cavitation extractor was proposed. Venturi tube was selected as the cavitation element, because it had better cavitation effect than orifice plate (Panda et al., 2020). The organic phase and aqueous phase collided at the T-shaped junction for the preliminary mixing. The violent mixing was obtained under the cavitation effect generated at the cavitation element. The full contact between aqueous phase and organic phase and the continuous renewal of two-phase interface contributed to the realization of efficient mass transfer process.

In this work, the removal of Fe^{3+} from 24% MAP solution by 2% D2EHPA in kerosene was investigated in the impact-jet HC extractor. The purpose of this work is to investigate the influence of cavitation effect on the removal of Fe^{3+} in MAP solution, explore the mechanism of Fe^{3+} extraction by D2EHPA, and seek a new method for impurity removal in phosphate industry.

2. Experimental section

2.1. Materials

Ammonium dihydrogen phosphate (AR grade) was provided by Damao Chemical Reagent Factory, China. Ferric ammonium sulfate dodecahydrate (AR grade) was obtained from Shanghai Chemical Reagent Co., Ltd., China. D2EHPA (AR grade) and kerosene (AR grade) were produced by Luoyang Aoda Chemical Co., Ltd., which were employed as extractant and diluent, respectively. Pure water produced by a Milli-Q system (Millipore Co., Ltd., USA) was used to prepare the aqueous phase solutions.

2.2. Experimental process parameters

24% MAP solution containing 0.01% Fe^{3+} was used as the aqueous phase, and 2% D2EHPA in kerosene was used as the organic phase. Before conducting the experiment, the aqueous phase and organic phase were preheated to the reaction temperature respectively. The parameters and conditions selected in the experiments were as follows: the concentration of D2EHPA, 0.5–4%; pH of initial MAP solution, 1.5–3.5; phase ratio of aqueous to organic (A/O), 0.5–4; extraction temperature, 303–343 K; extraction time 1–9 min; inlet pressure, 0.05–0.3 MPa.

2.3. Experimental device and setup

Fig. 1 shows the schematic diagram of the impact-jet HC extractor. The device had two inlets with the inner diameter

Table 1 Substances extracted by HC devices.

Extract	Source of extract	HC device	Operating conditions	Yield	Researchers
Protein	Soybean	Venturi	Inlet pressure: 100 MPa	82%	Preece et al. (2017)
Lipids	Microalgae Nannochloropsis salina	Venturi	Cv = 1.17; Extraction time: 25.05 min	25.9–99.0%	Lee and Han (2015)
Lipids	Microalgae Nannochloropsis salina	Orifice	Cv = 1.01 ~ 3.37; Extraction time: 20 min	46.0 ± 3.7%	Lee et al. (2019)
Enzyme	Yeast	Orifice	Pressure: 0.6 MPa; Temperature: 50 ℃	55.78 U/mL	Mevada et al. (2019)

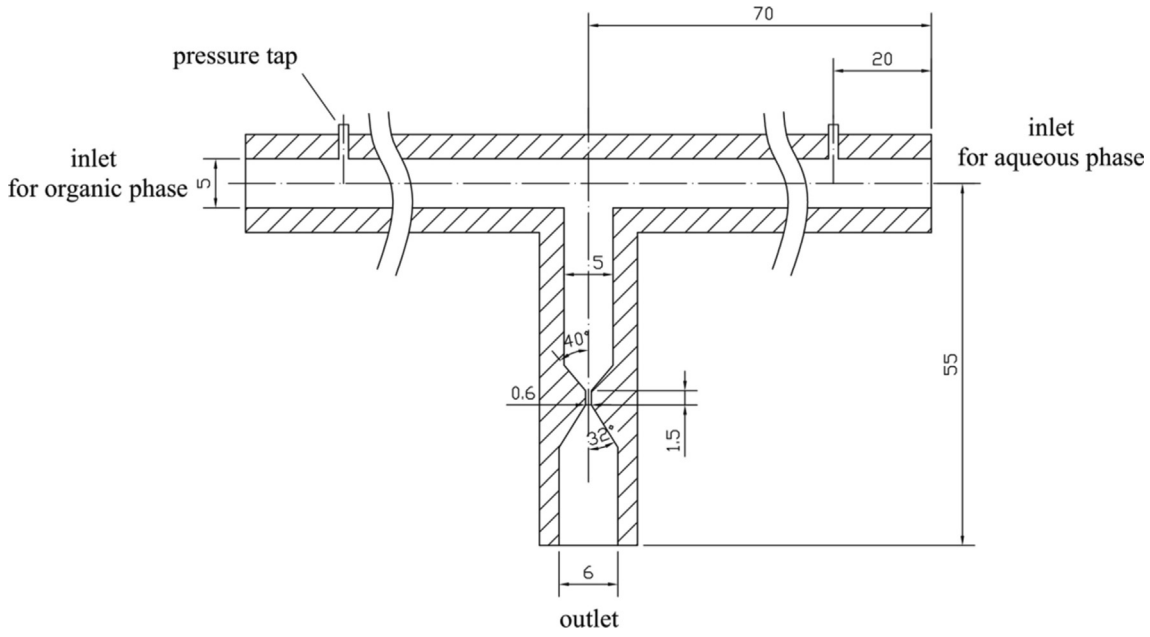

Fig. 1 Schematic diagram of the impact-jet HC extractor. (The unit of length is mm.)

of 5 mm and one outlet with the inner diameter of 6 mm. The two inlets were opposite and each was at an angle of 90° to the outlet. The core element of the device was the venturi as the cavitation element. The throat diameter of the venturi was 0.6 mm, the throat length was 1.5 mm, the inlet cone angle was 40°, and the outlet cone angle was 32°. The device was fabricated by machining technology, and it was made of polymethyl methacrylate (PMMA) which had excellent characteristics of transparency and easy processing.

The schematic diagram of the impact-jet hydraulic cavitation setup used in this work is shown in Fig. 2. The organic phase and aqueous phase were delivered respectively by two gear pumps (WT3000-1JB, Longer Precision Pump Co., Ltd.). The pressure of the pipe was controlled by adjusting the speed of the gear pumps, and the pressure values were displayed on the pressure gauges (Y-40Z, Hongqi Instrument Co., Ltd.) in real time. The fluids of organic phase and aqueous phase collided at the T-shaped junction for the preliminary mixing and then entered the venturi. Cavitation occured at the end of venturi throat and the expanding section. Due to the cavitation effect, the aqueous phase and the organic phase were highly mixed and the mass transfer conducted. The two-phase mixed fluids flew out of the venturi and into the beaker for cyclic extraction. After the cyclic extraction was completed, the raffinate solution in the lower part of the beaker was quickly transferred into a high-speed centrifuge (H1850, Xiangyi Centrifuge Instrument Co., Ltd.) and centrifuged at the centrifugal speed of 8000 r/min for 3 min. The mass transfer was prevented due to the complete separation of aqueous phase and organic phase. During the experiment, the temperature of the two-phase solution was accurately controlled by a constant-temperature water bath (DF-101S, Gongyi Yuhua Instrument Co., Ltd.). In addition, due to the density differences between organic phase and aqueous phase, the pipes for organic phase and aqueous phase were placed on the upper part and lower part of the beaker, respectively. When the operation was stable, the images of two-phase fluids mixing from the T-shaped junction to the end of venturi expanding section were obtained by a camera (X-T20, Fuji Photo Film Co., Ltd.), as shown in Fig. 3. The organic phase was close to the pipe wall, and the aqueous phase in a helical shape was wrapped by the organic phase and occupied the center of the pipe. When the two-phase fluids flew out of the venturi throat, the highly dispersed water-in-oil emulsion was generated instantly and filled the whole expanding section of venturi due to the cavitation effect. The morphology of the MAP crystals precipitated from the aqueous solution was observed by electron microscope (DM2000 LED, Leica-

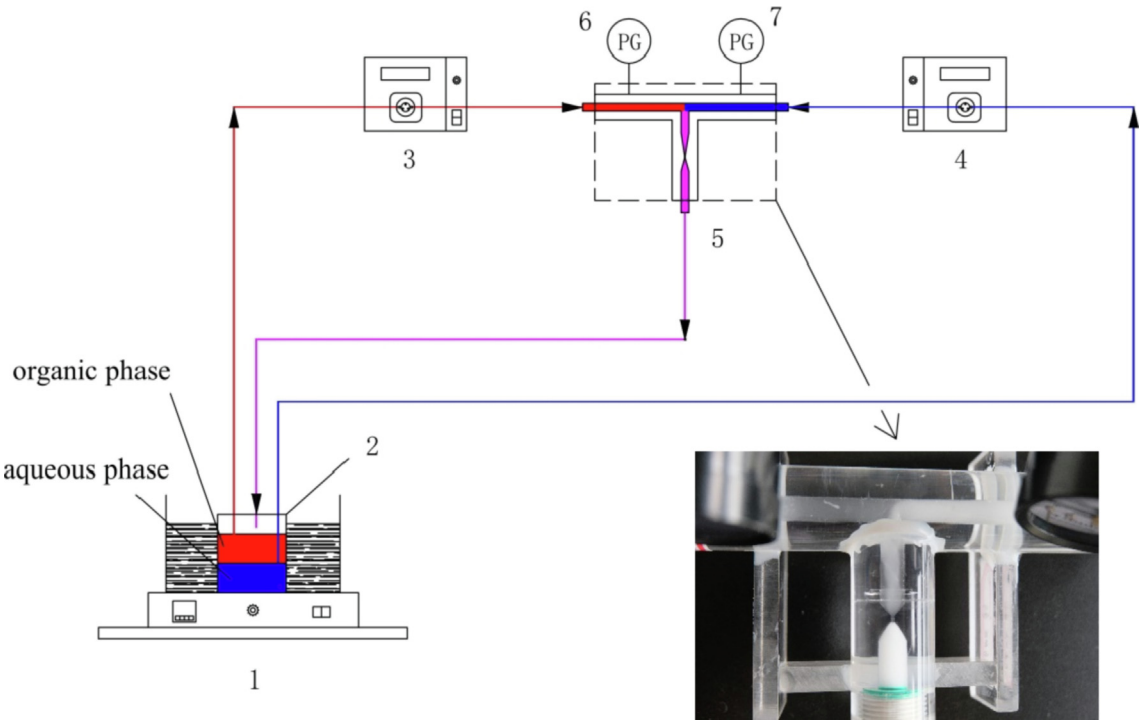

Fig. 2 Schematic diagram of the experimental setup: (1) constant-temperature water bath, (2) beaker, (3) gear pump for organic phase, (4) gear pump for aqueous phase, (5) impact-jet HC extractor, (6) and (7) pressure gauges.

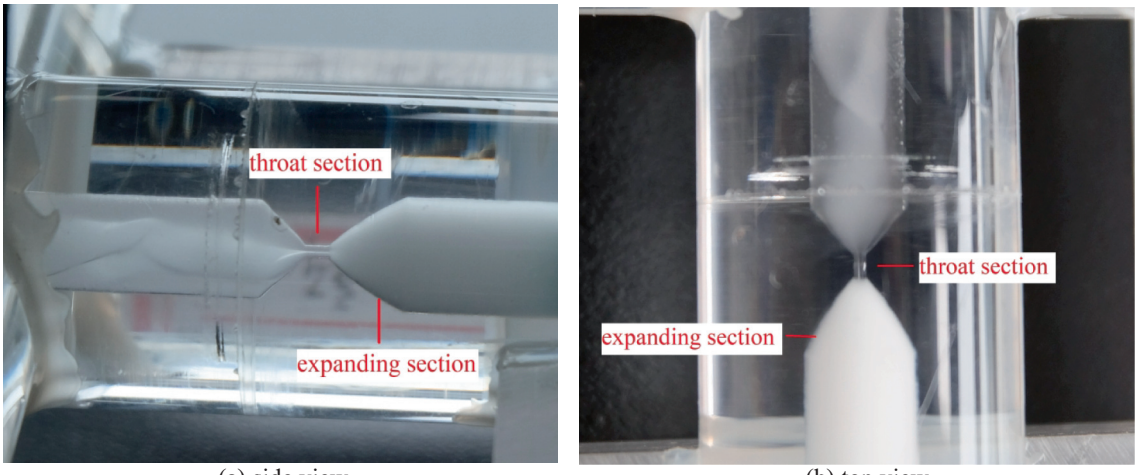

(a) side view (b) top view

Fig. 3 Images of two-phase fluids mixing from the T-shaped junction to the end of venturi expanding section (the images taken under the operation condition: P_{in} = 0.2 MPa, A/O = 1:1).

microsystems, Germany). The optical properties of MAP crystals was studied by X-ray diffractometer (D8A A25, Bruker, Germany) and ultraviolet–visible spectrometer (UV-2600, Shimadzu Co., Ltd.).

(No dye was used during the experiments, and the colors in the figure only indicated different fluids.)

2.4. Experimental analysis

The concentration of Fe^{3+} in aqueous phase was analyzed by the ultraviolet–visible spectrophotometry, in which the absorbance value was obtained at the wavelength of 510 nm (Luo et al., 2013).

3. Results and discussion

The degree of solute transferred from aqueous phase to organic phase can be reflected by extraction efficiency (ψ_E) (Dai et al., 2017) which is defined as follows:

$$\psi_E = \frac{C_{aqu,i} - C_{aqu,r}}{C_{aqu,i}} \times 100\% \quad (1)$$

where $C_{aqu,i}$ is the initial concentration of Fe^{3+} in aqueous phase. $C_{aqu,r}$ is the concentration of Fe^{3+} in the raffinate solution. Since the concentration of Fe^{3+} is very low, it can be approximately considered that the volume of organic phase and aqueous phase is unchanged before and after extraction.

3.1. Comparison of conventional stirring extraction and HC extraction

The conventional stirring extraction was performed in a beaker of 300 mL, where 100 mL of the aqueous phase was mixed with 100 mL of organic phase. The two phases were stirred at a speed of 400 r/min. Meanwhile, the HC extraction was carried out with the same system under the condition of the inlet pressure of 0.2 MPa for comparison. The results were shown in Fig. 4. When the extraction time was 5 min, the extraction efficiency of Fe^{3+} was 79.05% in HC extractor and the extraction of Fe^{3+} was basically saturated, while the extraction efficiency of Fe^{3+} was only 51.20% in conventional stirring device. The saturation point was reached at 40 min for conventional stirring extraction. Therefore, the faster extraction can be achieved in the HC extractor compared with the conventional stirring device. It was because that it was difficult to fully mix the organic phase and the aqueous phase under the conventional stirring conditions. However, under the action of hydraulic cavitation, the strong shock wave and high-speed micro-jet flow were generated, which can make the organic phase and aqueous phase highly mixed. Moreover, the cyclic extraction made the organic phase and aqueous phase undergo the action of multiple cavitation in a certain time, and the two-phase interface was constantly updated.

3.2. Effect of throat diameter

Cavitation number (C_v) (Petkovšek et al., 2013; Shah et al., 1999) is an important dimensionless number for HC device, which can reflect the strength of the cavitation effect. The smaller the value of C_v, the better the cavitation effect. The cavitation number can be defined as follows:

$$C_v = \frac{P_\infty - P_v}{\frac{1}{2}\rho u^2} \tag{2}$$

where P_∞ is the fully recovered downstream pressure of the cavitation element, P_v is the saturated vapor pressure of the liquid at operating temperature, u is the average velocity of the liquid at the throat of the cavitation element, and ρ is the density of the liquid.

α is a geometrical parameter, which is the ratio of the throat perimeter to the cross-sectional area of the throat (Panda et al., 2020). For the HC device used in this work, α can be calculated by the following formula:

$$\alpha = \frac{\pi d}{\frac{\pi}{4}d^2} = \frac{4}{d} \tag{3}$$

where d is the throat diameter. Bargole et al. (2019) pointed out that the higher cavitational yield can be achieved by the increase of α value.

For HC device, the cavitation effect is closely related to the extraction performance, and the throat diameter of the cavitation element has a direct impact on the cavitation effect. Therefore, the experiments were conducted by using the impact-jet HC extractor with the throat diameter of 0.6 mm and 0.8 mm, and the influence of throat diameter on extraction efficiency was discussed. The results were shown in Fig. 5.

A higher extraction efficiency was obtained in the HC extractor with 0.6 mm throat diameter. The extraction efficiency of the HC extractor with 0.6 mm throat diameter was 3.7–6.0% higher than that with 0.8 mm throat diameter. According to Eq. (2), the smaller the throat diameter of the HC extractor, the greater the average velocity of the fluid at the throat, and the smaller the value of C_V. According to Eq. (3), the smaller the throat diameter of the HC extractor, the higher the value of α. The decease of the value of C_V and the increase of the value of α indicated that the cavitation effect was enhanced. As a consequence, the mixing of the aqueous phase and organic phase was strengthened, so that the contact area of the two phases was increased and the mass transfer was enhanced.

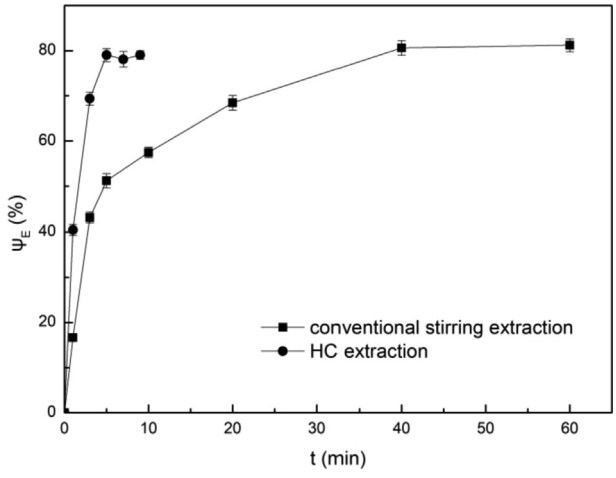

Fig. 4 Comparison of conventional stirring extraction and HC extraction. Conditions: A/O = 1:1, pH = 3.5, $C_{(HD)2}$ = 2%, T = 303 K.

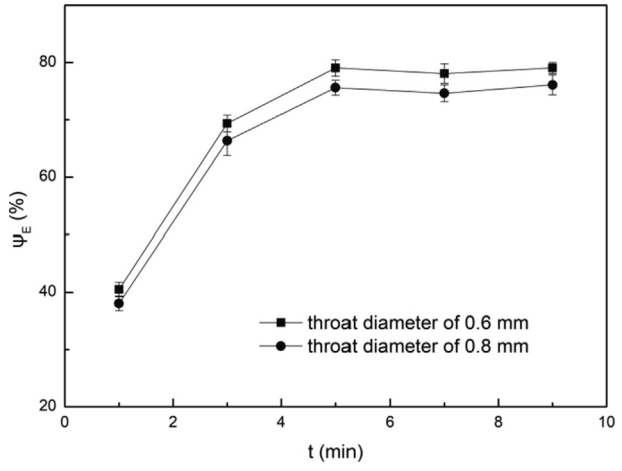

Fig. 5 Influence of throat diameter on extraction efficiency. Conditions: A/O = 1:1, pH = 3.5, $C_{(HD)2}$ = 2%, T = 303 K, P_{in} = 0.2 MPa.

3.3. Effect of phase ratio

Phase ratio (A/O) refers the ratio of aqueous phase volume to organic phase volume, which is an important factor for the extraction process. The change of phase ratio involves the change of extractant dosage. As the total amount of organic phase and aqueous phase remains unchanged, the change of the amount of organic phase has a significant impact on the extraction process. In order to further explore the effect of phase ratio on the extraction of Fe^{3+}, a parameter ξ_v has been introduced, which is the extraction capacity of the organic phase per unit volume to solutes. It can be defined as follows:

$$\xi_v = \frac{C_{aqu,i}V_{aqu} - C_{aqu,r}V_{aqu}}{V_{org}} \quad (4)$$

where V_{org} *and* V_{aqu} are the volumes of the organic phase and the aqueous phase, respectively. The effect of phase ratio on extraction efficiency was discussed, as shown in Fig. 6.

As phase ratio changed from 1:2 to 4:1, the extraction efficiency decreased almost linearly, and the highest extraction efficiency was obtained at the phase ratio of 1:2, which was 84.85%. This was because that with the increase of the phase ratio, the amount of extractant decreased and the extraction capacity was greatly weakened. It can be seen from Fig. 6 that ξ_v increased with the increase of phase ratio, which indicated that the extraction capacity of the extractant per unit volume increased. It can be explained that under the action of cavitation, the contact opportunity and contact surface between organic phase per unit volume and water phase were greater with the increase of phase ratio. The change of phase ratio had little effect on the C_v, which indicated that the cavitation intensity was basically unchanged. Therefore, the effect of phase ratio on extraction efficiency was mainly caused by the change of the amount of extractant.

3.4. Effect of inlet pressure

HC is caused by the change of pressure when the fluid passes through the contraction channel (such as orifice plate, venturi, etc.) (Carpenter et al., 2016, 2017). The pressure variations can cause the formation, growth and collapse of cavitation bubbles, which leads to the severe mechanical effects (such as shock wave and micro jet) and free radical effect. Therefore, pressure is an important factor affecting the cavitation effect which is closely related to the extraction efficiency. In this experiment, the influence of inlet pressure on extraction efficiency was studied as the outlet pressure was maintained at atmospheric pressure. The results were shown in Fig. 7.

As the inlet pressure increased from 0.05 MPa to 0.3 MPa, the extraction efficiency increased first and then decreased, and the highest extraction efficiency was achieved at the inlet pressure of 0.2 MPa. The inlet pressure of the cavitation element was determined by the flow rate of the fluids at the throat of the element. With the increase of inlet pressure, the velocity of fluids passing through the throat of the venturi increased. According to Eq. (2), the value of C_V decreased, which indicated that the cavitation effect was enhanced. When the inlet pressure was increased to a certain level, the velocity of cavitation bubbles passing through the cavitation zone was very fast and the residence time was quite short. As a result, the cavitation bubbles collapsed before it grew large enough, which reduced the collapse intensity of cavitation bubbles and the cavitation effect was weakened (Buffo and Reineccius, 2002). Therefore, the optimum inlet pressure for the extraction of Fe^{3+} was 0.2 MPa.

3.5. Effect of temperature

Distribution ratio (D) is a vital parameter in the solvent extraction, which can indicate the degree of solute transferred between different phases. It can be defined as follows:

$$D = \frac{C_{iron,org}}{C_{iron,aqu}} \quad (5)$$

where $C_{iron,org}$ and $C_{iron,aqu}$ are the concentration of Fe^{3+} in organic phase and aqueous phase, respectively.

In this experiment, the effect of temperature on the extraction of Fe^{3+} was investigated at 303, 313, 323, 333 and 343 K, and lg$D$ was plotted with $(1/T) \times 10^{-3}$, as shown in Fig. 8.

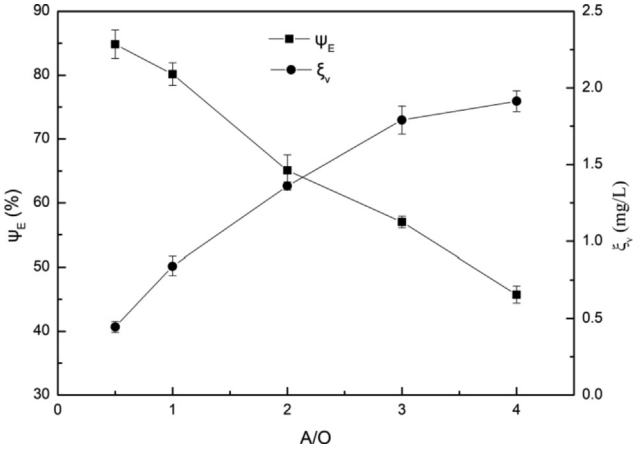

Fig. 6 Influence of phase ratio on extraction efficiency. Conditions: pH = 3.5, $C_{(HD)2}$ = 2%, T = 303 K, P_{in} = 0.2 MPa, t = 5 min.

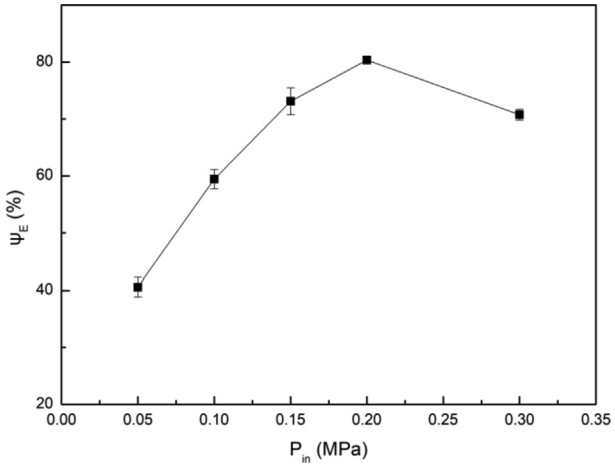

Fig. 7 Influence of inlet pressure on extraction efficiency. Conditions: A/O = 1:1, pH = 3.5, $C_{(HD)2}$ = 2%, T = 303 K, t = 5 min.

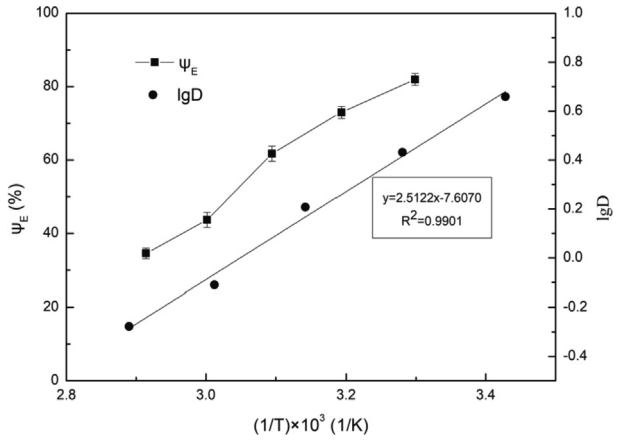

Fig. 8 Influence of temperature on extraction efficiency. Conditions: A/O = 1:1, pH = 3.5, $C_{(HD)2}$ = 2%, P_{in} = 0.2 MPa, t = 5 min.

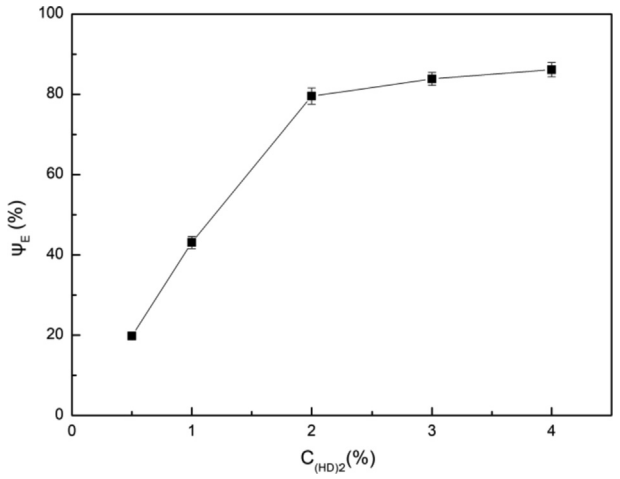

Fig. 9 Influence of D2EHPA concentration on extraction efficiency. Conditions: A/O = 1:1, pH = 3.5, T = 303 K, P_{in} = 0.2 MPa, t = 5 min.

With the increase of temperature, both the extraction efficiency and distribution ratio decreased significantly, and a linear relation of lg$D$ and $(1/T) \times 10^{-3}$ was obtained. Based on the Van't Hoff equation (Otu and Chiarizia, 2001), the following relation can be established:

$$\lg D = \frac{-\Delta H}{2.303RT} + C \tag{6}$$

where △H is enthalpy change and C is a constant. The △H value can be calculated for −48.1 kJ/mol, which indicated that the extraction of Fe^{3+} with D2EHPA was an exothermic reaction. Thus, the extraction of Fe^{3+} can be inhibited with the increase of temperature. In addition, with the increase of temperature, the saturated vapor pressure of liquid increased. Thus, the C_v decreased and the cavitation effect increased. It can be explained that the enhancement of cavitation effect was less than the inhibition of extraction of Fe^{3+} due to the increase of temperature, so the extraction efficiency and distribution ratio decreased with the increase of temperature.

3.6. Effect of D2EHPA concentration

D2EHPA is usually complexed with metal ions in the form of dimer (Dai et al., 2017), which can be abbreviated as $(HD)_2$. The effect of D2EHPA concentration on extraction efficiency was studied, as shown in Fig. 9. The extraction efficiency increased obviously with the increase of the concentration (mass fraction) of D2EHPA from 0.5% to 2%, while the extraction efficiency remained almost unchanged with the increase of the D2EHPA concentration from 2% to 4%. It was indicated that the extraction of Fe^{3+} with 2% D2EHPA was almost saturated. The trend reflected in Fig. 9 was consistent with the trend that the extraction efficiency of Mg^{2+} changed with D2EHPA volume fraction provided by Luo et al. (2011)

3.7. Effect of pH of initial MAP solution

Since D2EHPA (H_2D_2) contains dissociatable H^+, the mechanism of extracting Fe^{3+} with D2EHPA may be the cation exchange (Van de Voorde et al., 2005). The equilibrium equation of extracting Fe^{3+} with D2EHPA can be described as follows:

$$xFe^{3+}_{(aqu)} + \frac{(q+m)x}{2}(HD)_{2(org)} = (FeD_q \cdot mHD)_{x(org)} + qxH^+_{(aqu)} \tag{7}$$

According to Eq. (7), the equilibrium constant (K) can be expressed as follows:

$$K = \frac{[(FeD_q \cdot mHD)_x]_{(org)} \cdot [H^+]^{qx}_{(aqu)}}{[Fe^{3+}]^x_{(aqu)} \cdot [(HD)_2]^{\frac{(q+m)x}{2}}_{(org)}} \tag{8}$$

It is assumed that iron exists only in the form of Fe^{3+} and $(FeD_q{\cdot}mHD)_x$ in the aqueous phase and organic phase ,respectively. The concentration of iron in the aqueous phase and organic phase can be expressed respectively as follows:

$$C_{iron,aqu} = [Fe^{3+}]_{(aqu)} \tag{9}$$

$$C_{iron,org} = x\,[(FeD_q \cdot mHD)_x]_{(org)} \tag{10}$$

Combing Eq. (8) with Eq. (5), Eq. (9) and Eq. (10), the following relation can be obtained

$$\lg D = \lg K + qxpH + \lg x + (x - 1)\lg[Fe^{3+}]_{aqu} + \frac{(q+m)x}{2}\lg[(HD)_2] \tag{11}$$

The effects of pH and extractant concentration on extraction equilibrium were studied by the slope method, respectively. The relationships of lgD and pH as well as lgD and lg $[(HD)_2]$ were obtained, as shown in Fig. 10 and Fig. 11, respectively. It can be seen from Fig. 10 that the extraction efficiency increased with the increase of pH. It was because that the concentration of H^+ decreased with the increase of pH, which was conducive to the extraction of Fe^{3+}. This was consistent with the cation exchange mechanism reflected in Eq. (7). According to the charge conservation in Eq. (7) and the slope values of 0.6341 and 1.6379 obtained in Fig. 10 and Fig. 11, the equilibrium equation of extracting Fe^{3+} with D2EHPA can be expressed as follows:

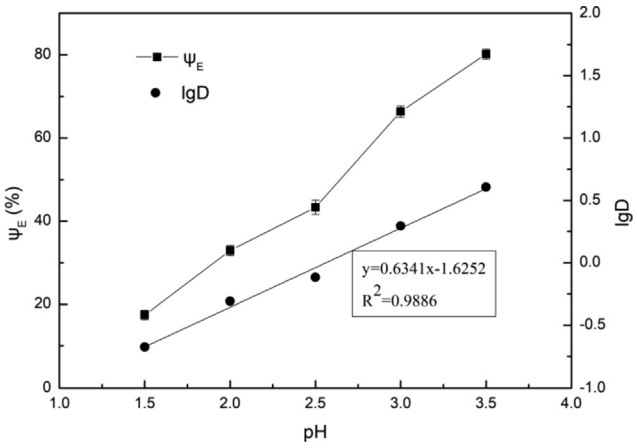

Fig. 10 Influence of pH on extraction efficiency. Conditions: A/O = 1:1, $C_{(HD)2}$ = 2%, T = 303 K, P_{in} = 0.2 MPa, t = 5 min.

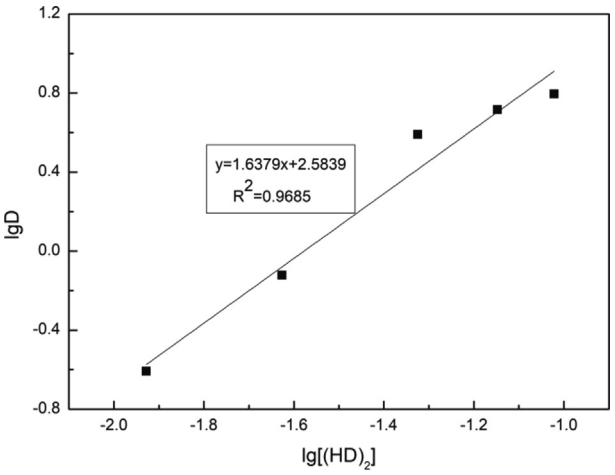

Fig. 11 Relationship of lgD and lg[$(HD)_2$]. Conditions: A/O = 1:1, pH = 3.5, T = 303 K, P_{in} = 0.2 MPa, t = 5 min.

$$Fe^{3+}_{(aqu)} + 8(HD)_{2(org)} = (FeD_3 \cdot 13HD)_{(org)} + 3H^{+}_{(aqu)} \quad (12)$$

It can be seen that the Fe^{3+} was transferred to the organic phase and existed in the form of complex of FeD_3·13HD. The schematic diagram of the extraction process was illustrated in Fig. 12.

3.8. Two-stage extraction

The above studies showed that the good extraction of the extraction efficiency of about 80% can be achieved under the conditions that the throat diameter of the cavitation element was 0.6 mm, the phase ratio was 1:1, the inlet pressure was 0.2 MPa, the extraction temperature was 303 K, the concentration of D2EHPA was 2% and the pH of MAP solution was 3.5. The Fe^{3+} in MAP solution can be reduced from 100 ppm to about 20 ppm. The two-stage extraction, in which the raffinate after the one-stage extraction was extracted with the same concentration of organic phase, was carried out. The result was shown in Fig. 13. The concentration of Fe^{3+} was reduced to 3.4 ppm, the total extraction efficiency reached 96.7%.

3.8.1. Electron microscopic study

The crystal morphology of MAP without impurities was polyhedral structure (Davey and Mullin, 1974; Xue et al., 2005). The existence of Fe^{3+} in MAP solution can seriously affect the growth rate and growth morphology of crystals. Barrett et al. (1989) pointed out that the change of crystal growth rate and crystal morphology can be affected by two aspects. On the one hand, the Fe^{3+} adsorbed on the crystal surface can hinder the growth of the crystal. On the other hand, the existence of Fe^{3+} can break the hydrogen bonds and cause the lattice strain, which can inhibit the growth of the crystal and cause the change of crystal morphology. In this study, the morphology of the precipitated crystals from the initial aqueous solution, raffinate solution after the one-stage extraction, raffinate solution after the two-stage extraction and the solution of analytical-grade MAP was observed by electron microscope, as shown in Fig. 14. The morphology of the precipitated crystals from the initial MAP solution, which contained 100 ppm Fe^{3+}, was mainly rod-shaped structure with large length-to-diameter ratio, as shown in Fig. 14 (a). After the one-stage extraction, about 20 ppm Fe^{3+} remained in the raffinate solution. As shown in Fig. 14 (b), there were still a few rod-shaped crystals with large length-to-diameter ratio in the MAP crystals precipitated from the raffinate solution, which indicated that about 20 ppm Fe^{3+} still had a certain effect on the crystal morphology. The MAP crystals precipitated from the raffinate solution after the two-stage extraction were uniform in size and regular in structure, which was generally close to the regular polyhedral structure of crystals of analytical-grade MAP. It was illustrated that it was effective to remove Fe^{3+} from MAP solution based on the HC technol-

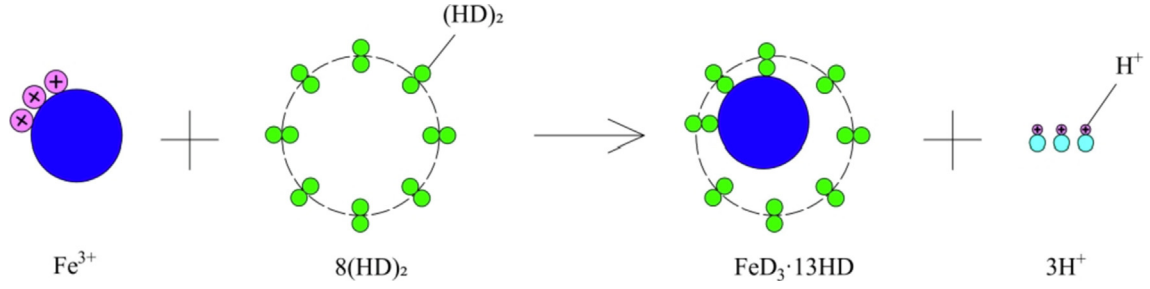

Fig. 12 Schematic diagram of the extraction of Fe^{3+} with D2EHPA.

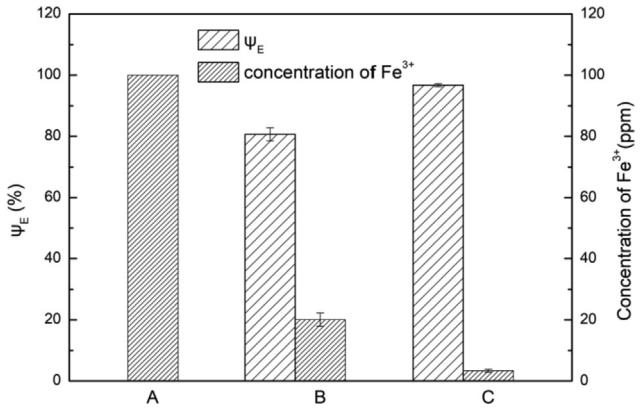

Fig. 13 Influence of extraction times on extraction efficiency (A: initial MAP solution; B: raffinate after one-stage extraction; C: raffinate after two-stage extraction). Conditions: A/O = 1:1, pH of initial MAP solution = 3.5, $C_{(HD)2}$ = 2%, P_{in} = 0.2 MPa, t = 5 min.

ogy, and higher-quality MAP products can be obtained after two-stage extraction.

3.8.2. Powder XRD study

Two samples of crystals precipitated from the initial MAP solution with 100 ppm Fe^{3+} and precipitated from the raffinate solution with 4 ppm Fe^{3+} were obtained. The powder XRD patterns of the two samples were compared. The results were shown in Fig. 15. It can be seen that the XRD patterns of MAP crystals with different contents of Fe^{3+} were basically the same, and both the samples had the characteristic diffraction peaks of MAP. No additional phase was observed, which indicated the MAP crystals were single phase nature. The result was consistent with the result reported by Dhanalakshmi et al. (2020). In general, there was a slight higher diffraction peak intensity for the sample with 4 ppm Fe^{3+} compared with that with 100 ppm Fe^{3+}, and there was almost no jump in the position of the diffraction peaks of the two samples. This results were also shown with expanded scale in Fig. 16. The change of diffraction peak intensity was caused due to the different contents of Fe^{3+} in the MAP crystals (Joshi et al., 2020). The shifting of diffraction peaks can be caused by the lattice strain (Joshi et al., 2018; Vanchinathan et al., 2012). There was no jump in the position of the diffraction peaks in this study. It may be that the Fe^{3+} adsorbed on the crystal surface in the form of hydrated ions $Fe(H_2O)_6^{3+}$ only caused the change of the crystal growth rate and didn't destroy the hydrogen bond, and the lattice strain was not caused (Barrett et al., 1989). It can be inferred that the change of the MAP crystal morphology (as shown in Fig. 14) was mainly caused by the change of crystal growth rate which was led to by the Fe^{3+} adsorbed on the crystal surface.

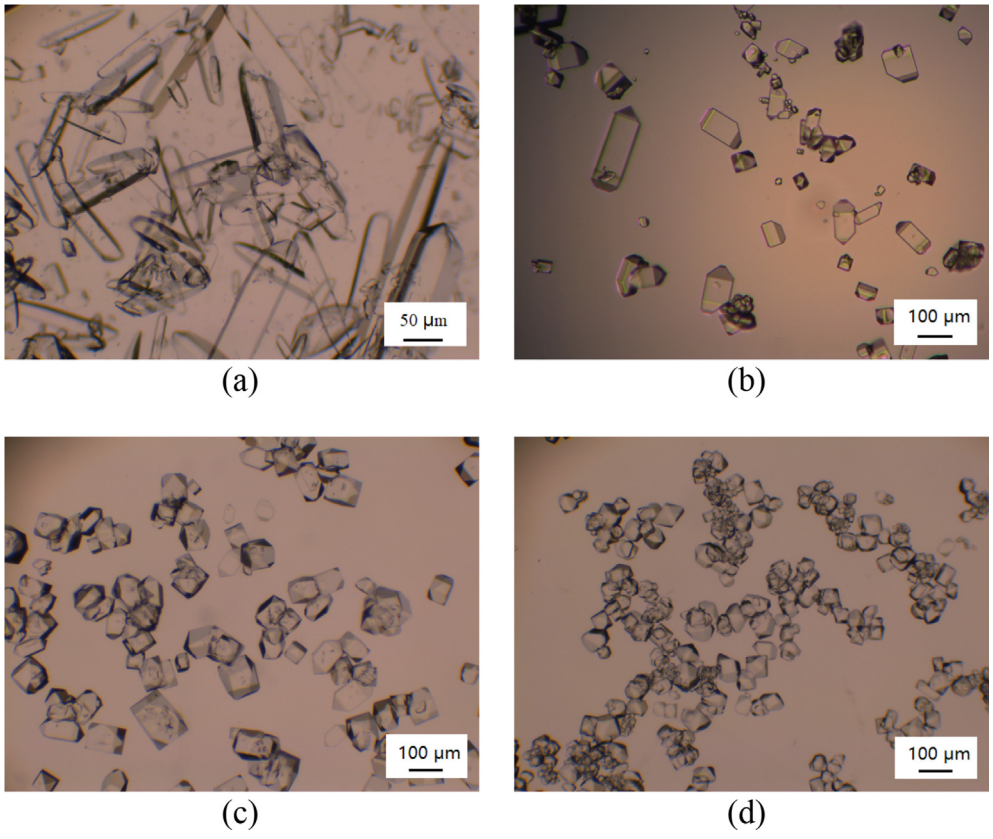

Fig. 14 Morphology of MAP crystals obtained from aqueous solutions containing different Fe^{3+} concentrations. (A: initial MAP solution with 100 ppm Fe^{3+}; B: raffinate solution containing 19.4 ppm Fe^{3+} after one-stage extraction; C: raffinate solution containing 3.4 ppm Fe^{3+}after two-stage extraction; D: analytical-grade MAP solution).

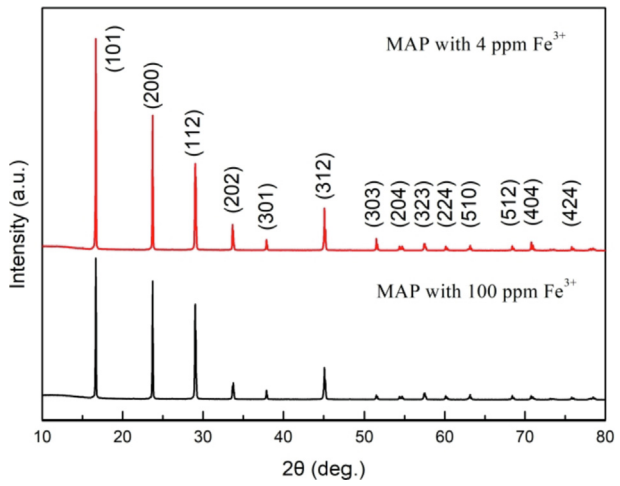

Fig. 15 Powder XRD patterns of crystals precipitated from the initial MAP solution with 100 ppm Fe^{3+} and precipitated from the raffinate solution with 4 ppm Fe^{3+}.

3.8.3. UV–Vis spectroscopy study

The UV–Visible transmittance spectra can be used to investigate the linear optical properties of grown crystals (Joshi et al., 2019a, 2019b, 2020). In this study, the effect of the impurity of Fe^{3+} on the optical transmittance of MAP was studied by the UV–Visible transmittance spectra. The result was shown in Fig. 17. It can be seen that both samples (MAP with 100 ppm Fe^{3+} and MAP with 4 ppm Fe^{3+}) showed the nearly 100% maximal transmittance in entire visible range. Furthermore, throughout the wavelengths of the UV region, the optical transmittance increased with the increase of the wavelength, and the MAP with 4 ppm Fe^{3+} showed higher transmittance than that with 100 ppm Fe^{3+}. It was indicated that the removal of impurity of Fe^{3+} from MAP solution was conducive to improve the optical transmittance of MAP crystal. The result showed a good agreement with the result of Feng et al. (2016) who pointed out that the decrease of Fe^{3+} in materials contributed to the increase of transmittance

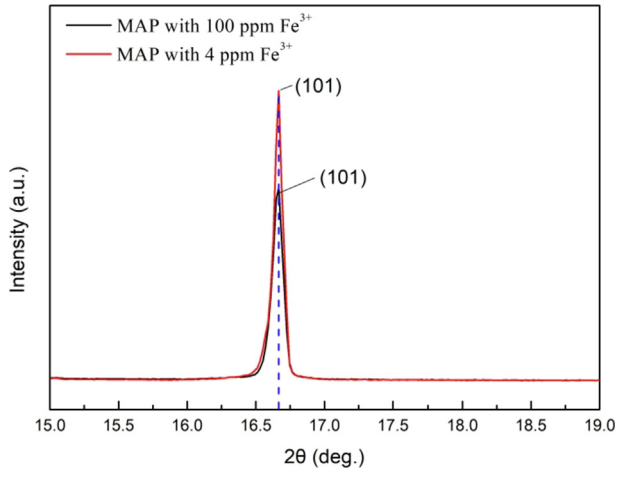

Fig. 16 (101) Diffraction peak of crystals precipitated from the initial MAP solution with 100 ppm Fe^{3+} and precipitated from the raffinate solution with 4 ppm Fe^{3+}.

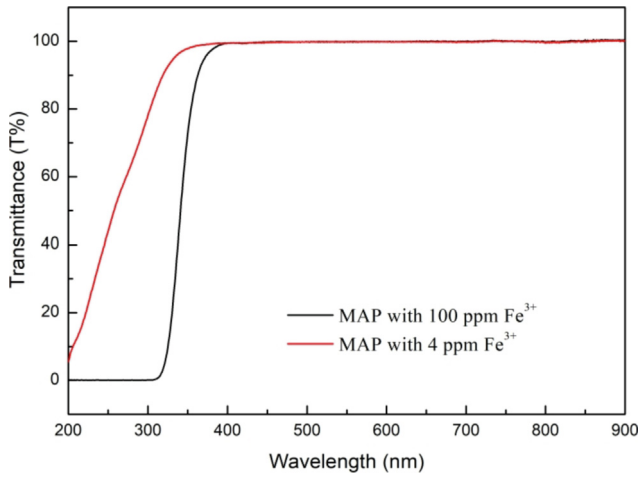

Fig. 17 UV–Visible transmittance spectra of MAP with 100 ppm Fe^{3+} and MAP with 4 ppm Fe^{3+}.

of most wavelengths. Therefore, the removal of Fe^{3+} from MAP solution by hydraulic cavitation technology is conducive to expand the application of MAP in the field of optoelectronics.

4. Conclusions

The removal of Fe^{3+} from the MAP solution by D2EHPA was investigated in an impact-jet hydraulic cavitation extractor. The effects of various parameters including throat diameter, phase ratio, inlet pressure, temperature, D2EHPA concentration, and pH of initial MAP solution on extraction efficiency were investigated. It was found that the organic phase and aqueous phase can be highly mixed under the action of hydraulic cavitation. The extraction efficiency of 80% can be achieved by one-stage extraction for 5 min. The greater cavitation effect can be obtained with the decrease of throat diameter, which conducive to the improvement of extraction efficiency. The optimum inlet pressure for the extraction of Fe^{3+} was 0.2 MPa. The increase of D2EHPA concentration and pH was benefit for the extraction of Fe^{3+}, while the extraction was inhibited by the increase of phase ratio and temperature. The results indicated that the extraction of Fe^{3+} with D2EHPA was an exothermic reaction. The equilibrium equation of extraction was obtained by slope method as follows:

$$Fe^{3+}_{(aqu)} + 8(HD)_{2(org)} = (FeD_3 \cdot 13HD)_{(org)} + 3H^{+}_{(aqu)}$$

The extraction efficiency of up to 96.7% can be reached by two-stage extraction in the impact-jet HC extractor. Electron micrograph showed that the regular polyhedral structure of MAP crystals were obtained. The powder XRD indicated the single phase nature of MAP crystals and there was no lattice strain caused by the impurity of Fe^{3+}. The UV–Visible transmittance spectra indicated that the removal of Fe^{3+} from MAP solution was beneficial for the increase of optical transmittance of MAP crystals. The results were shown that the higher-quality MAP products can be obtained by the hydraulic cavitation technology. This paper provides a new liquid–liquid extraction method for the removal of impurities in phosphate industry based on the hydraulic cavitation technology.

Data availability

The data that support the findings of this study are available from the corresponding author upon reasonable request.

Declaration of Competing Interest

The authors declare that they have no known competing financial interests or personal relationships that could have appeared to influence the work reported in this paper.

Acknowledgement

This work was supported by the National Natural Science Foundation of China (31660472); Middle-aged and Young Teachers' Basic Ability Promotion Project of Guangxi (2020KY08027); and the Project of Science and Technology Base and Talent of Guangxi (Guike AD20238033).

References

Bargole, S., George, S., Saharan, V.K., 2019. Improved rate of transesterification reaction in biodiesel synthesis using hydrodynamic cavitating devices of high throat perimeter to flow area ratios. Chem. Eng. Process. Process Intensif. 139, 1–13. https://doi.org/10.1016/j.cep.2019.03.012.

Barrett, N.T., Lamble, G.M., Roberts, K.J., Sherwood, J.N., Greaves, G.N., Davey, R.J., Oldman, R.J., Jones, D.J., 1989. Glancing angle EXAFS investigation of the habit modification of ADP by the incorporation of iron. J. Cryst. Growth. 94 (3), 689–696. https://doi.org/10.1016/0022-0248(89)90093-6.

Buffo, R.A., Reineccius, G.A., 2002. Modeling the rheology of concentrated beverage emulsions. J. Food Eng. 51 (4), 267–272. https://doi.org/10.1016/S0260-8774(01)00067-X.

Carpenter, J., Badve, M., Rajoriya, S., George, S., Saharan, V.K., Pandit, A.B., 2016. Hydrodynamic cavitation: An emerging technology for the intensification of various chemical and physical processes in a chemical process industry. Rev. Chem. Eng. 33 (5), 1–36. https://doi.org/10.1515/revce-2016-0032.

Carpenter, J., George, S., Saharan, V.K., 2017. Low pressure hydrodynamic cavitating device for producing highly stable oil in water emulsion: Effect of geometry and cavitation number. Chem. Eng. Process. Process Intensif. 116, 97–104. https://doi.org/10.1016/j.cep.2017.02.013.

Dai, S., Luo, J.H., Li, J., Zhu, X.H., Cao, Y., Komarneni, S., 2017. Liquid−liquid microextraction of Cu^{2+} from water using a new circle microchannel device. Ind. Eng. Chem. Res. 56, 12717–12725. https://doi.org/10.1021/acs.iecr.7b01888.

Davey, R.J., Mullin, J.W., 1974. Growth of the 101 faces of ammonium dihydrogen phosphate crystals in the presence of ionic specie. J. Cryst. Growth. 23 (2), 89–94. https://doi.org/10.1016/0022-0248(74)90106-7.

Dhanalakshmi, M., Parthiban, S., Swaminathan, M., 2020. Crystal growth and optical properties of ammonium dihydrogen phosphate (ADP) crystals doped with Fe(II) and Fe(III): Oxidation number effects. *Mater. Today. P.* 29 (4), 1119-1124. https://doi.org/10.1016/j.matpr.2020.05.200.

El-Bayaa, A.A., Badawy, N.A., Gamal, A.M., Zidan, I.H., Mowafy, A.R., 2011. Purification of wet process phosphoric acid by decreasing iron and uranium using white silica sand. J. Hazard. Mater. 190 (1–3), 324–329. https://doi.org/10.1016/j.jhazmat.2011.03.037.

Fan, C.X., Ma, R., Wang, Y.B., Luo, J.H., Komarneni, S., 2020. Gas-liquid-liquid flow patterns and extraction in a rotating microchannel extractor. Can. J. Chem. Eng. 99 (S1), S668–S680. https://doi.org/10.1002/cjce.23975.

Feng, X., Zhu, L.L., Li, F.Q., Wang, F., Han, W., Wang, Z.P., Zhu, Q.H., Sun, X., 2016. Growth and highly efficient third harmonic generation of ammonium dihydrogen phosphate crystals. Rsc Adv. 6 (40), 33983–33989. https://doi.org/10.1039/C6RA02283A.

Gupta, D.K., Chatterjee, S., Datta, S., Veer, V., Walther, C., 2014. Role of phosphate fertilizers in heavy metal uptake and detoxification of toxic metals. Chemosphere. 108, 134–144. https://doi.org/10.1016/j.chemosphere.2014.01.030.

Joshi, J.H., Dixit, K.P., Parikh, K.D., Jethva, H.O., Kanchan, D.K., Kalainathan, S., Joshi, M.J., 2018. Effect of Sr^{2+} on growth and properties of ammonium dihydrogen phosphate single crystal. J. Mater. Sci-mater. El. 29 (7), 5837–5852. https://doi.org/10.1007/s10854-018-8556-8.

Joshi, J.H., Kalainathan, S., Joshi, M.J., Parikh, K.D., 2020a. Crystal growth, spectroscopic, second and third order nonlinear optical spectroscopic studies of L-phenylalanine doped ammonium dihydrogen phosphate single crystals. Arab. J. Chem. 13 (4), 5018–5026. https://doi.org/10.1016/j.arabjc.2020.01.024.

Joshi, J.H., Kalainathan, S., Joshi, M.J., Parikh, K.D., 2019a. Influence of l-serine on microstructural, spectroscopic, electrical and nonlinear optical performance of ammonium dihydrogen phosphate single crystal. J. Mater. Sci-mater. El. 30 (4), 14243–14255. https://doi.org/10.1007/s10854-019-01793-0.

Joshi, J.H., Kalainathan, S., Kanchan, D.K., Joshi, M.J., Parikh, K. D., 2019b. Crystal growth, A.C. electrical and nonlinear optical studies of pure and dl-methionine doped ammonium dihydrogen phosphate single crystals. J. Mater. Sci.-Mater. El. 30, 2985–2993. https://doi.org/10.1007/s10854-018-00577-2.

Joshi, J.H., Kalainathan, S., Kanchan, D.K., Joshi, M.J., Parikh, K. D., 2020b. Effect of L-threonine on growth and properties of ammonium dihydrogen phosphate crystal. Arab. J. Chem. 13 (1), 1532–1550. https://doi.org/10.1016/j.arabjc.2017.12.005.

Kong, L.Z., Guan, H., Wang, X.Q., 2018. In situ polymerization of furfuryl alcohol with ammonium dihydrogen phosphate in poplar wood for improved dimensional stability and flame retardancy. ACS Sustain. Chem. Eng. 6 (3), 3349–3357. https://doi.org/10.1021/acssuschemeng.7b03518.

Lampila, L.E., 2013. Applications and functions of food-grade phosphates. Ann. N.Y. Acad. Sci. 1301 (1), 37–44. https://doi.org/10.1111/nyas.12230.

Lee, I., Han, J., 2015. Simultaneous treatment (cell disruption and lipid extraction) of wet microalgae using hydrodynamic cavitation for enhancing the lipid yield. Bioresour. Technol. 186, 246–251. https://doi.org/10.1016/j.biortech.2015.03.045.

Lee, I., Oh, Y., Hanc, J., 2019. Design optimization of hydrodynamic cavitation for effectual lipid extraction from wet microalgae. J. Environ. Chem. Eng. 7, (2). https://doi.org/10.1016/j.jece.2019.102942 102942.

Li, W.Q., Liu, H., Li, J., You, C.X., 2020. Mass transfer process study of Fe(III) extraction from ammonium dihydrogen phosphate solution. J. Ser. Chem. Soc. 85 (8), 1055–1065. https://doi.org/10.2298/JSC191017032L.

Lo, T.C., Baird, M.H., Hanson, C., 1983. Handbook of Solvent Extraction. Wiley, New York.

Luo, J.H., Li, J., Duan, X.X., Jin, Y., 2013. Extraction of Fe^{3+} from sodium dihydrogen phosphate with colloidal liquid aphrons. Ind. Eng. Chem. Res. 52 (11), 4306–4311. https://doi.org/10.1021/ie3031899.

Luo, J.H., Li, J., Jin, Y., Zhang, Y., Zheng, D.S., 2009. Study on Mg^{2+} removal from ammonium dihydrogen phosphate solution by predispersed solvent extraction. Ind. Eng. Chem. Res. 48 (4), 2056–2060. https://doi.org/10.1021/ie801277t.

Luo, J.H., Li, J., Wang, B.M., 2014. Study on Mg^{2+} removal from ammonium dihydrogen phosphate solution by an emulsion liquid membrane. Hem. Ind. 68 (3), 341–346. https://doi.org/10.2298/HEMIND130511058L.

Luo, J.H., Li, J., Zhou, K., Jin, Y., 2011. Study on Mg^{2+} removal from ammonium dihydrogen phosphate solution by solvent

extraction with di-2-ethylhexyl phosphoric acid. Korean J. Chem. Eng. 28 (4), 1105–1109. https://doi.org/10.1007/s11814-010-0468-0.

Maddikeri, G.L., Gogate, P.R., Pandit, A.B., 2014. Intensified synthesis of biodiesel using hydrodynamic cavitation reactors based on the interesterification of waste cooking oil. Fuel. 137, 285–292. https://doi.org/10.1016/j.fuel.2014.08.013.

Mevada, J., Devi, S., Pandit, A., 2019. Large scale microbial cell disruption using hydrodynamic cavitation: Energy saving options. Biochem. Eng. J. 143, 151–160. https://doi.org/10.1016/j.bej.2018.12.010.

Mohammad, I., Khaiary, E.I., 1997. Extraction of Al(III) from phosphoric acid by HDDNSA. Sep. Sci. Technol. 12 (1), 13–16. https://doi.org/10.1016/S1383-5866(97)00004-X.

Otu, E.O., Chiarizia, R., 2001. Thermodynamics of the extraction of metal ions by dialkyl-substituted diphosphonic acids. II. The U(VI) and Sr(II) case. Solvent Extr. Ion Exc. 19 (6), 1017–1036. https://doi.org/10.1081/SEI-100107617.

Panda, D., Manickam, S., 2018. Sonochemical degradation of endocrine-disrupting organochlorine pesticide Dicofol: Investigations on the transformation pathways of dechlorination and the influencing operating parameters. Chemosphere. 204, 101–108. https://doi.org/10.1016/j.chemosphere.2018.04.014.

Panda, D., Manickam, S., 2019. Hydrodynamic cavitation assisted degradation of persistent endocrine-disrupting organochlorine pesticide Dicofol: Optimization of operating parameters and investigations on the mechanism of intensification. Ultrason. Sonochem. 51, 526–532. https://doi.org/10.1016/j.ultsonch.2018.04.003.

Panda, D., Saharan, V.K., Manickam, S., 2020. Controlled hydrodynamic cavitation: A review of recent advances and perspectives for greener processing. Processes. 8 (2), 220. https://doi.org/10.3390/pr8020220.

Petkovšek, M., Zupanc, M., Dular, M., Kosjek, T., Heath, E., Kompare, B., širok, B.,, 2013. Rotation generator of hydrodynamic cavitation for water treatment. Sep. Purifi. Technol. 118, 415–423. https://doi.org/10.1016/j.seppur.2013.07.029.

Preece, K.E., Hooshyar, N., Krijgsman, A.J., Fryer, P.J., Zuidam, N. J., 2017. Intensification of protein extraction from soybean processing materials using hydrodynamic cavitation. Innov. Food Sci. Emerg. Technol. 41, 47–55. https://doi.org/10.1016/j.ifset.2017.01.002.

Rajoriya, S., Bargole, S., Saharan, V.K., 2017. Degradation of reactive blue 13 using hydrodynamic cavitation: Effect of geometrical parameters and different oxidizing additives. Ultrason. Sonochem. 37, 192–202. https://doi.org/10.1016/j.ultsonch.2017.01.005.

Ramisetty, K.A., Pandit, A.B., Gogate, P.R., 2014. Novel approach of producing oil in water emulsion using hydrodynamic cavitation reactor. Ind. Eng. Chem. Res. 53 (42), 16508–16515. https://doi.org/10.1021/ie502753d.

Saxena, S., Saharan, V.K., George, S., 2018. Enhanced synergistic degradation efficiency using hybrid hydrodynamic cavitation for treatment of tannery waste effluent. J. Clean. Prod. 198, 1406–1421. https://doi.org/10.1016/j.jclepro.2018.07.135.

Shah, Y.T., Pandit, A.B., Moholkar, V.S., 1999. Cavitation Reaction Engineering. Kluwer, New York.

Vanchinathan, K., Muthu, K., Bhagavannarayana, G., Meenakshisundaram, S.P., 2012. Growth of cerium(III)-doped ADP crystals and characterization studies. J. Cryst. Growth. 354 (1), 57–61. https://doi.org/10.1016/j.jcrysgro.2012.05.012.

Van de Voorde, I., Pinoy, L., Courtijn, E., Verpoort, F., 2005. Influence of acetate ions and the role of the diluents on the extraction of copper (II), nickel (II), cobalt (II), magnesium (II) and iron (II, III) with different types of extractants. Hydrometallurgy. 78 (1–2), 92–106. https://doi.org/10.1016/j.hydromet.2005.02.008.

Xue, D.F., Ratajczak, H., 2005. Effect of hydrogen bonds on physical properties of ammonium dihydrogenphosphate crystals. *J. Mol. Struc.-theochem.* 716 (1-3), 207-210. https://doi.org/10.1016/j.theochem.2004.11.026.

Yan, J.C., Ai, S., Yang, F., Zhang, K.M., Huang, Y.C., 2020. Study on mechanism of chitosan degradation with hydrodynamic cavitation. Ultrason. Sonochem. 64,. https://doi.org/10.1016/j.ultsonch.2020.105046 105046.

Zhu, X.H., Li, J., Jin, Y., Guo, Y.H., 2017. Preparation of porous hybrid adsorbents based on fluor(calcium silicate)/activated carbon and its application in the removal of iron (III) from ammonium phosphate solutions. Arab. J. Chem. 13 (1), 1551–1562. https://doi.org/10.1016/j.arabjc.2017.12.006.